JOINT EUROPEAN TORUS

JET–P(88)50

A. Gondhalekar, A.D. Cheetham, J.C.M. de Haas, A. Hubbard,
P.D. Larsen, J. O'Rourke, M. Watkins and JET Team

Simultaneous Measurements of Electron Thermal and Particle Transport in JET

Simultaneous Measurements of Electron Thermal and Particle Transport in JET

A. Gondhalekar, A.D. Cheetham, J.C.M. de Haas[1], A. Hubbard,
P.D. Larsen, J. O'Rourke, M. Watkins and JET Team*

JET-Joint Undertaking, Culham Science Centre, OX14 3DB, Abingdon, UK

[1]FOM Instituut voor Plasmafysica "Rijnhuizen", The Netherlands.
** See annex of P. Lallia et al, "Plasma Heating in JET",*
(13th EPS Conference on Controlled Fusion and Plasma Physics, Schliersee, Germany (1986)).

Preprint of Paper to be submitted for publication in
Plasma Physics and Controlled Fusion

Simultaneous Measurements of Electron Thermal and Particle Transport in *JET*

A Gondhalekar, A D Cheetham, J C M de Haas*, A Hubbard,
J O'Rourke and M L Watkins.

JET Joint Undertaking, Abingdon, OX14 3EA, UK.
*FOM Instituut voor Plasmafysica "Rijnhuizen", The Netherlands.

1. Introduction:

An important objective in tokamak research is to find suitable descriptions for the measured thermal and particle fluxes, and to identify the underlying mechanism of transport. Many detailed models for transport in tokamaks have been developed [1], which make specific predictions for the correlations between the thermal and particle transport coefficients. In order to exclude some of the contending models, accurate measurements of the correlations are required. In order to reduce uncertainties arising from shot-to-shot and spatial variations it is necessary to determine these coefficients simultaneously in the same spatial region of the plasma.

In this paper we describe evaluation of electron thermal and particle transport coefficients by three different methods satisfying the above requirements: (a) analysis of inward propagation of electron temperature and density perturbations produced when a small pellet is injected into the plasma; (b) measurements of the velocity and damping of electron temperature and density pulses propagating outwards following sawtooth collapse; (c) time dependent transport analysis applied to non-stationary plasmas.

In the following we present determinations of X_e and D_e for Ohmically heated deuterium plasmas in JET, limited by the outer carbon belt limiters, for the following range of parameters: I_ϕ = 3MA, $2.8 \le B_\phi(T) \le 3.4$, $1.5 \le \bar{n}_e(10^{19}\ m^{-3}) \le 2.7$, $T_e(0) \approx 3$ keV and $T_i(0) \approx 1.5$ keV.

2. Determination of X_e and D_e by Pellet Injection:

Local thermal and particle diffusivities can be determined by analysis of the propagation of electron temperature and density perturbations caused by injection of a small pellet into the plasma [2] such that it penetrates to the boundary of the plasma region best suited to this investigation, $0.5 \leq r/a \leq 0.8$, where a is the plasma minor radius. The analysis is performed in the region $r_c < r < r_p$, where r_p is the pellet penetration radius and r_c is the sawtooth inversion radius. Typically, in the investigations reported here, $0.3 \leq r_c/a \leq 0.5$ and $r_p/a \approx 0.7$. In previous investigations [3,4] we have shown that the radial propagation of electron temperature and density perturbations generated by pellet injection may be representative of the local transport properties of the target plasma.

X_e is determined by comparing the temporal evolution of the electron temperature profile in the region $r_c < r < r_p$, with a simulation using a diffusive model including sources,

$$(3/2)n_e(r)\ d(kT_e(r))/dt = -\ \mathrm{div}Q_e + S(r) \qquad \ldots 1.$$

where

$$Q_e = -X_e(r)\ n_e(r)\ \nabla(kT_e(r)) + Q_p \qquad \ldots 2.$$

Q_p is a thermal pinch flux

$S(r)$ is the thermal source

k is Boltzmann's constant.

Because the applied perturbation is small, the thermal pinch and source terms may be assumed to remain constant throughout the temperature profile evolution, allowing them to be combined into an effective source, $S_{eff}(r)$, so that eq.1 becomes

$$(3/2)n_e(r)d(kT_e(r))/dt = \mathrm{div}[X_e(r)n_e(r)\nabla(kT_e(r))] + S_{eff}(r)$$

where

$$S_{eff} = -\mathrm{div}Q_p + S(r)$$

$T_e(r,t)$ is deduced from measurements of electron cyclotron emission (ECE) using two instruments, a scanning Michelson interferometer (KK1), which gives a radial profile of T_e every ≈15ms, and a 12 channel grating polychromator (KK2) which measures the emission at 12 radial positions on a μs time scale. The electron density profile, $n_e(r)$, is constructed from far infra-red (0.195mm) interferometric measurements of line-integrated density along six vertical chords through a poloidal cross-section of the JET plasma. The source term $S_{eff}(r)$ is calculated for the equilibrium, pre-pellet plasma where $\dot{T}_e(r) = \dot{n}_e(r) = 0$. The initial condition for solving eq. 1, $T_e(r,t=0)$, $n_e(r,t=0)$, the temperature and density profiles instantly after pellet injection, are determined from measurements of $T_e(r)$, $n_e(r)$, pellet mass, ablation rate and penetration depth. The T_e and n_e profiles immediately before and after pellet injection are shown in fig. 1. The pellet deposition profile is deduced from a model calculation of the pellet ablation, the neutral gas and plasma shielding model [5,6] using as input the temperature and density profiles of the target plasma. The calculation reproduces both the pellet penetration, as seen by the soft x-ray cameras viewing the pellet trajectory, and the maximum in the deposition, as evidenced by the electron density profile measured immediately after pellet injection. The product $n_e(r)T_e(r)$ immediately before and after pellet injection agree within <10% over the profile, and $\int_0^a n_e(r)T_e(r)\, 2\pi r dr$ before and after pellet injection agree within <2%. During the evolution of $T_e(r,t)$ the perturbed density profile, fig. 1, is assumed to be stationary. This is justified because the density perturbation travels much more slowly than the temperature perturbation, as will become clear in the following. The source $S_{eff}(r)$ is also assumed to be unchanged; the pellet injection events chosen for this analysis are such that the perturbations in total radiated losses and ohmic input power are small.

The modelled $T_e(r,t)$ evolution in the region of interest is found to be sensitive to the local value of X_e. We assume $X_e(r) = X_o[1 + \alpha(r/a)^{\beta}]$, where α and β are such that in the measurement region X_e is nearly constant, and increases sharply in the outer region of the plasma. Such a form is suggested by power balance calculations. X_o is iterated until good agreement with the measured $T_e(r,t)$ is obtained. Fig. 2 shows a comparison of the measured and modelled $T_e(r,t)$ at three different radii $r<r_p$. A value of $X_e = 2.8 \pm 0.3\ m^2/s$ is deduced at $0.5 \le r/a \le 0.6$.

In an analagous manner D_e is determined by comparing the evolution of the electron density profile with a simulation using a diffusive model including sources,

$$dn_e(r)/dt = -\mathrm{div}\Gamma(r) + S_e(r) \qquad \ldots 3.$$

where

$$\Gamma(r) = -D_e(r)\, \nabla n_e(r) + \Gamma_p(r) \qquad \ldots 4.$$

$S_e(r)$ is the electron source

The pinch flux is expressed as $\Gamma_p = n_e(r)V_p(r)$. The diffusion coefficient is parameterised as $D_e(r) = D_o[1 + \alpha(r/a)^\beta]$, so that $D(r)$ is minimum in the core, and increases towards the plasma edge. This form for $D(r)$ is justified by our previous measurements of density profile dynamics in JET [7,8].

The electron source $S_e(r)$ is given by ionisation of neutral H/D in the plasma, the neutral density profile established by recycling at the plasma edge and penetration by multiple charge exchange. The neutral density profile is determined by a 1-d neutral transport code from which an electron source profile is deduced. The electron source profile is calibrated at the edge using the ionization rate determined from the absolute H_α/D_α measurement [7,8]. Spectroscopic measurements suggest that impurity ionization contributes half of the total electron source. This is taken into account by multiplying the H/D ionization source by a factor of two. The calculation of $D_e(r)$ is carried out as follows. $D_e(r)$ is specified for the equilibrium $n_e(r)$ before the perturbation. With the appropriate total $S_e(r)$, the pinch velocity $V_p(r)$ is self-consistently calculated. Using these values of $D_e(r)$, $V_p(r)$ and $S_e(r)$ the evolution of the perturbed $n_e(r,t)$ is calculated and compared with the measured $n_e(r,t)$. The value of D_o is iterated until a good match is achieved. The initial condition, $n_e(r,t=0)$, is determined as described earlier. For the same pulses analysed above for X_e, a value of $D_e = 0.4 \pm 0.1$ m²/s is deduced at $0.5 \leq r/a \leq 0.6$. The corresponding $V(r) \approx -V_o(r/a)^4$ with $V_o \approx 1$ m/s. These values are consistent with previous measurements [7,8]. The above determinations of X_e and D_e performed simultaneously for the same pellet event yield $X_e/D_e = 7.0 \pm 2.5$.

3. Determination of X_e and D_e from Sawtooth Propagation:

Here the temperature and density perturbations are caused by the naturally occurring sawteeth. The local electron thermal diffusivity X_e is determined by analysis of the electron temperature perturbation which takes the form of a heat pulse propagating outwards from the mixing radius (r_m) after a sawtooth collapse, a technique described in detail in [9]. $T_e(r,t)$ is determined using the KK2 instrument in which the electron temperature is deduced from measurements of electron cyclotron emission. Two parameters are derived, a heat pulse velocity and a damping rate of the pulse amplitude. X_e is determined by comparison with simulations of these parameters using a diffusive model including sources. The temperature and density profiles are measured immediately before the sawtooth crash. The initial condition for the temperature profile evolution is obtained by flattening the temperature profile to its value at the sawtooth inversion radius (r_c) out to the mixing radius such that the perturbation conserves energy: $\int_0^\infty \delta E(r)\ 2\pi r dr = 0$, as shown in fig. 3.

Equation 1 is solved, ignoring variations in density. This is justified since the thermal perturbation travels 5-10 times faster than the density perturbation, and the density perturbation is much smaller. Typically for the conditions studied here, $\delta T_e(0)/T_e(0) \approx 0.1$ and $\delta n_e(0)/n_e(0) \approx 0.02$. Furthermore the sources (and sinks) are assumed to remain unchanged during the pulse propagation. These assumptions reduce eq. 1 to a diffusion equation in the perturbed temperature only. Fig. 4 shows a comparison of the measured and modelled heat pulse propagation. Measurements are made in a region of the plasma bounded by the normalised minor radius $0.6 \le r/a \le 0.8$ and, to increase the signal to noise ratio of the KK2 instrument, averaged over several sawteeth for a period of $\le$1s. The model calculation is done in the JET plasma geometry and X_e is assumed constant over the measurement region. From the analysis of a number of discharges a value of $X_e = 2.9 \pm 0.4\ m^2/s$ is deduced.

The electron particle diffusivity D_e is determined in a similar manner by measuring the propagation of a density pulse following a sawtooth collapse, the density perturbation observed using a reflectometer, as discussed in detail in [10]. The diffusing perturbation is clearly seen at all positions outside the mixing radius (r_m). The delay time of the pulse to reach each position is compared with predictions of a diffusive model in which the equilibrium electron density profile is periodically flattened inside the mixing radius, in the same manner as done above for the electron temperature. The density pulse propagation is modelled using a diffusion coefficient D_e, a pinch flux $\Gamma_p = -D_e n_e r/a^2$ and an edge recycling coefficient $R \approx 1$. These parameters are all assumed to remain constant during the analysis which continues over several sawteeth, with periodic flattening of the density profile, until a quasi steady-state is attained. The value of D_e is iterated until the calculated delay of the density pulse matches the measured value in the region $r_m \le r \le 0.85a$. Analysis of the same discharges used above for the determination of X_e, gives $D_e = 0.4 \pm 0.2\ m^2/s$. The above determinations of D_e and X_e performed in the same discharges, covering the same spatial and temporal regions, yield $X_e/D_e = 7.3 \pm 3.2$.

4. Determination of X and D_e from time dependent transport analysis:

Thermal and particle transport in JET have been described by expressions of the form [11,7]

$$Q(r) = -X(r)n(r)\nabla T(r) + Q_p(r) \qquad ...5.$$

$$\Gamma_e(r) = -D_e(r)\nabla n_e(r) + \Gamma_p(r) \qquad ...6.$$

Where Q and Γ_e are the heat and particle fluxes
X and D_e are the diffusivities
Q_p and Γ_p are the convective (pinch) fluxes

From these equations we infer that a plot of Q_e vs $-n\nabla T$ has a slope of X and an intercept of Q_p. Similarly D_e and Γ_p can be determined. Such 'flux gradient' analysis has been carried out for steady state heat fluxes for plasmas under various conditions [11]. This technique has been applied to transient conditions by plotting successive time points, yielding the particle transport coefficients. The transient is induced by injecting a small pellet. Analysis of such discharges yields $D_e = 0.4$ (+0.2,-0.1) m^2/s and $-\Gamma_p = 1.4$ (+5,-0.5) $x10^{18}$ $/m^2.s$.

5. Conclusions:

Table 1 summarizes the results of all the measurements described in sections 2,3 and 4. The measurements yield $X_e = 2.9\pm0.4$ m^2/s and $D_e = 0.4\pm0.2$ m^2/s, giving $X_e/D_e = 7.2 \pm 3$ at $0.5\leq r/a\leq 0.7$ in Ohmically heated deuterium plasmas, limited by the outer carbon belt limiters, with parameters I_ϕ = 3MA, $2.8 \leq B_\phi(T) \leq 3.4$, and $1.5 \leq \bar{n}_e(10^{19}\ m^{-3}) \leq 2.7$. Efforts are in progress to determine X_i directly by a method analagous to that described in section 2, using pellet injection. Propagation of an ion temperature perturbation is measured, as evidenced by neutron emission perturbations viewed by a multi-chord neutron camera.

Table 1.

Method	χ_e (m^2/s)	D_e (m^2/s)	$-\Gamma_p$ (10^{18} $m^{-2}s^{-1}$)
(a)	2.8 ± 0.3	0.4 ± 0.1	2.0 ± 0.7
(b)	2.9 ± 0.4	0.4 ± 0.2	-
(c)	-	$0.4^{+0.2}_{-0.1}$	$1.4^{+5}_{-0.5}$

Where (a) Pellet Injection: $0.5 \leq r/a \leq 0.6$

(b) Heat and density pulse following sawteeth: $0.6 \leq r/a \leq 0.8$

(c) Time dependent transport analysis: $r/a \approx 0.7$

Acknowledgement:

The authors would like to thank D Garton for computational support. Part of the work discussed in this paper makes use of data obtained during pellet injection experiments performed under a collaboration agreement between the JET Joint Undertaking and the US Department of Energy.

References:

[1] J D Callen, JET Report JET-IR(87)07.

[2] A Gondhalekar,et al., 15th Euro. Conf. on Controlled Fusion and Plasma Physics, Dubrovnik, 1988. Europhys. Conf. Abstracts Vol 12B, part I, p.151.

[3] A D Cheetham, et al., 14th Euro. Conf. on Controlled Fusion and Plasma Physics, Madrid, 1987. Europhys. Conf. Abstracts Vol 11D, part I, p.205.

[4] A D Cheetham, et al., Proc. International School of Plasma Physics, Varenna 1986. CEC Publication EUR 10797 EN, vol.2, 681.

[5] A Gondhalekar, et al., 11th IAEA Conf on Plasma Physics and Controlled Nuclear Fusion Research, Kyoto 1986. Proceedings, Vol 3, p.457.

[6] M L Watkins, et al., 14th Euro. Conf. on Controlled Fusion and Plasma Physics, Madrid, 1987. Europhys. Conf. Abstracts Vol 11D, part I, p.201.

[7] A Gondhalekar, et al., Bull. Am. Phys. Soc.30 (1985) 1525 and JET Report JET-P(85)31.

[8] A D Cheetham, et al., 13th Euro. Conf. on Controlled Fusion and Plasma Physics, Schliersee, 1986. Europhys Conf. Abstracts Vol 10C, part I, p.240.

[9] B J D Tubbing, et al., Nuclear Fusion 27 (1987) 1843, and N J Lopes-Cardozo, et al., Nuclear Fusion 28 (1988) 1173.

[10] A Hubbard, et al., 13th Euro. Conf. on Controlled Fusion and Plasma Physics, Schliersee, 1986. Europhys. Conf. Abstracts Vol 10C, part I, p.232.

[11] J D Callen et al., Nuclear Fusion 27 (1987) 1857.

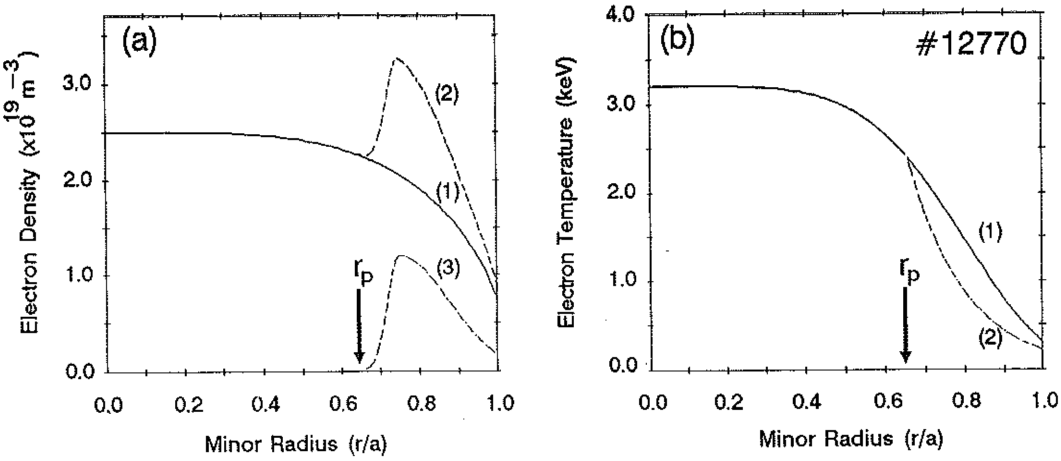

Fig. 1 (a) Pre-pellet radial profile of the electron density (1); the pellet deposition profile (3); and the total post-pellet density profile (2). (b) Pre-pellet radial electron temperature profile (1) and post-pellet T_e profile (2). The profiles (a2) and (b2) are the initial conditions for the transport calculation.

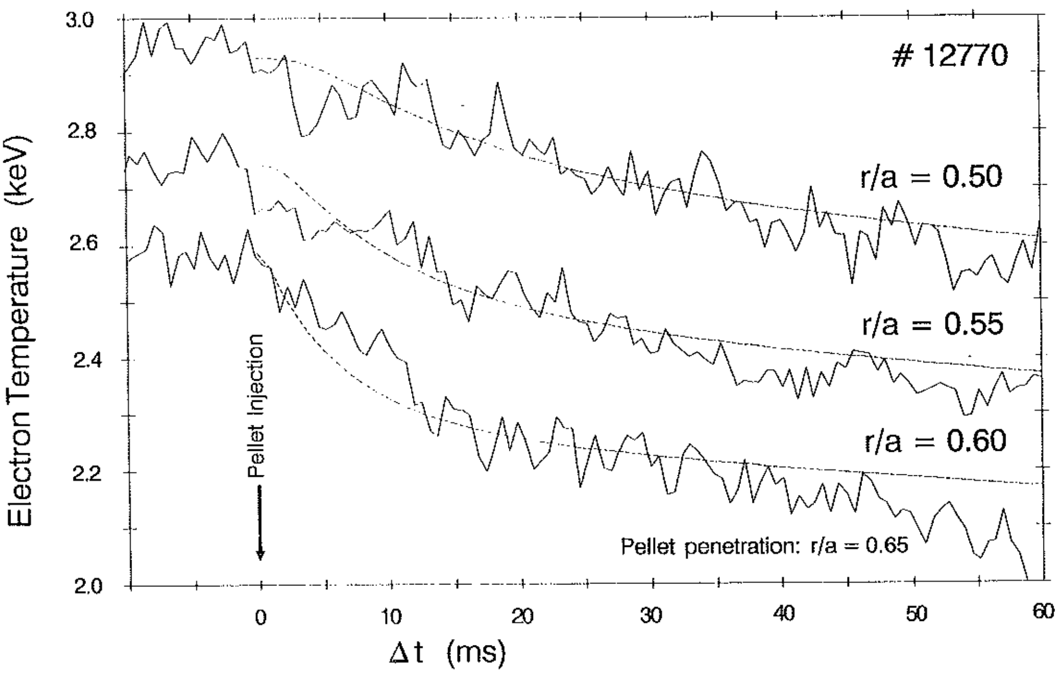

Fig. 2 The temporal evolution of the electron temperature at different radii (r/a) after injection of a pellet. The full line is the measured T_e, and the dashed line is the modelled evolution.

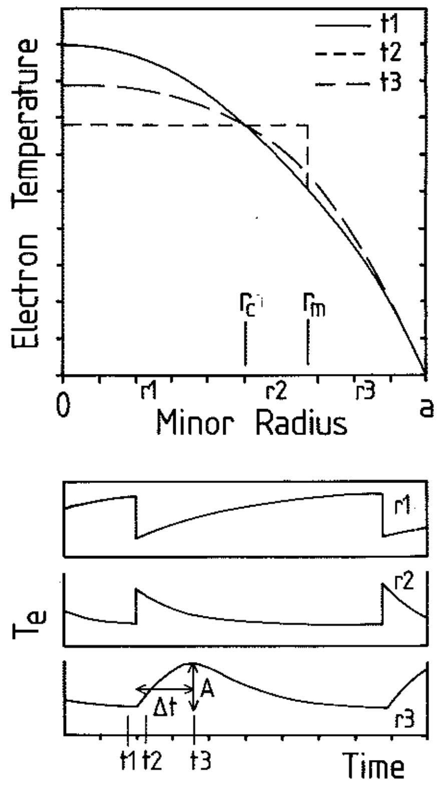

Fig. 3 Electron temperature evolution during a sawtooth crash: at times, t1- pre-crash, t2- initial condition for the simulation, t3- post-crash; and at three radii, $r1 \langle r_c$, $r_c \langle r2 \langle r_m$, $r3 \rangle r_m$. Where r_c is the sawtooth inversion radius and r_m is the mixing radius. A is the amplitude and Δt the time delay of the heat pulse.

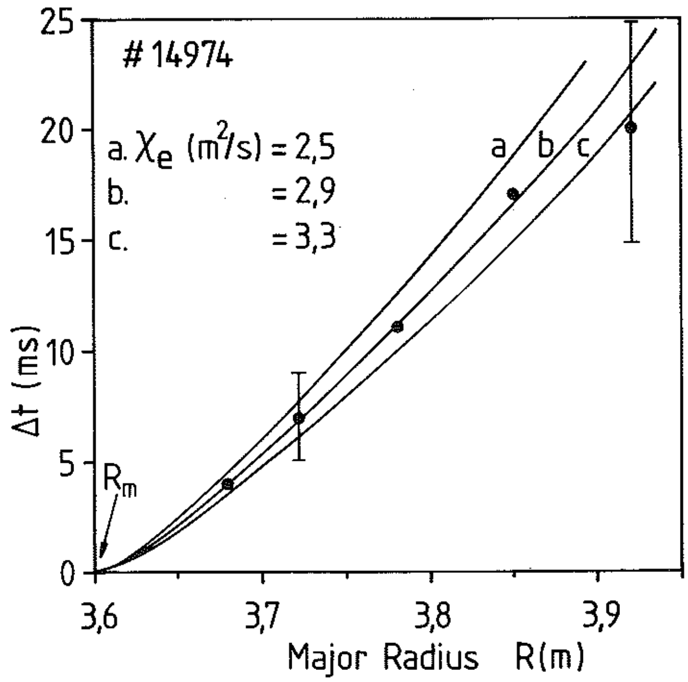

Fig. 4 Comparison of the measured and modelled time for arrival of the peak of the heat pulse, Δt(ms), following a sawtooth crash vs. the major radius R. R_m is the position of the mixing radius. The sensitivity of the model calculation to errors in the input parameters is indicated.